POLYBRICK 2.0

Bio-Integrative Load Bearing Structures

Eda Begum Birol*
Yao Lu*
Ege Sekkin*
JSLab, Department
of Architecture, AAP,
Cornell University

* Authors contributed equally

Colby Johnson
David Moy
Yaseen Islam
Department of Mechanical
Engineering, Cornell University

Jenny Sabin
JSLab, Department
of Architecture, AAP,
Cornell University

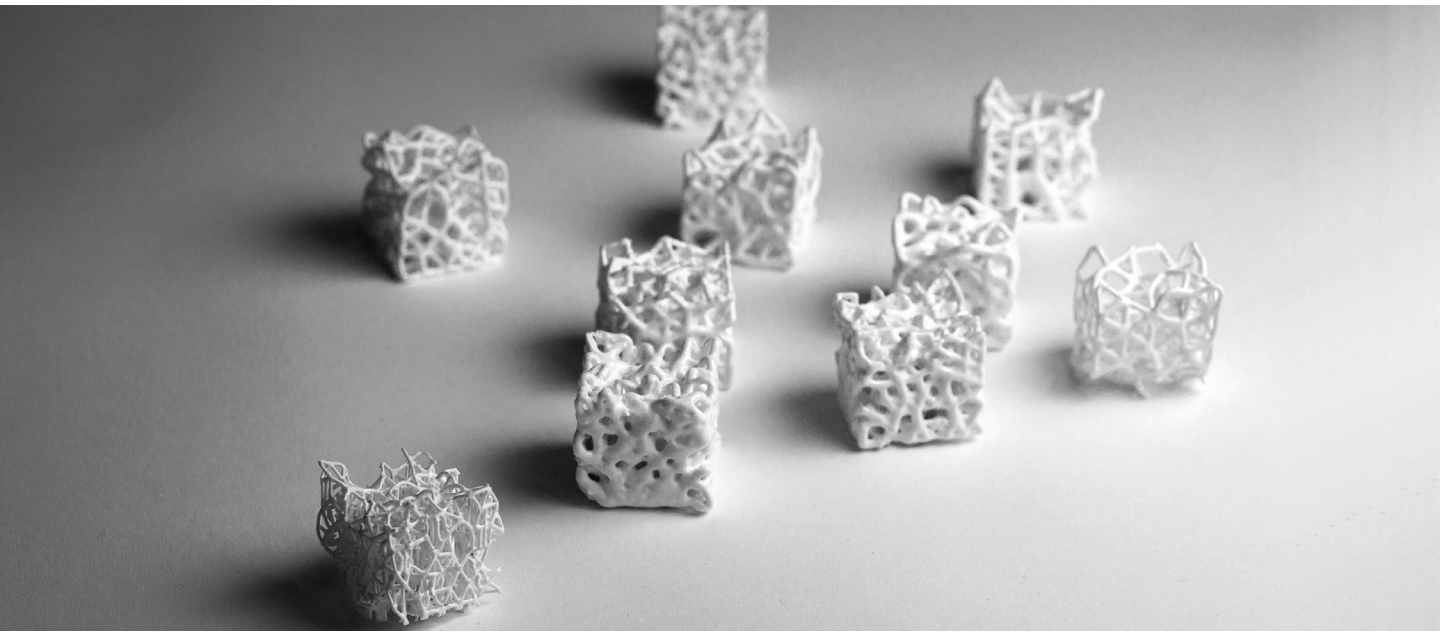

1

ABSTRACT

Natural load bearing structures are characterized by aspects of specialized morphology, lightweight, adaptability, and a regenerative life cycle. PolyBrick 2.0 aims to learn from and apply these characteristics in the pursuit of revitalizing ceramic load bearing structures. For this, algorithmic design processes are employed, whose physical manifestations are realized through available clay/porcelain additive manufacturing technologies (AMTs). By integrating specialized expertise across disciplines of architecture, engineering, and material science, our team proposes an algorithmic toolset to generate PolyBrick geometries that can be applied to various architectural typologies. Additionally, comparative frameworks for digital and physical performance analyses are outlined. Responding to increasing urgencies of material efficiency and environmental sensibility, this project strives to provide for designers a toolset for environmentally responsive, case-specific design, characterized by the embedded control qualities derived from the bone and its adaptability to specific loading conditions. Various approaches to brick tessellation and assembly are proposed and architectural possibilities are presented.
As an outcome of this research, PolyBrick 2.0 is effectively established as a Grasshopper plug-in, "PolyBrick" to be further explored by designers.

1 Various PolyBrick 2.0 prototype geometries: Fabrication is carried through with aid of Formlabs Form 2 ceramic resin printer, prototypes are then bisque fired at cone 06 and glaze fired at cone 4 in medium speed.

INTRODUCTION

"Ceramic modules of standard measurement have been used as a building block [...] for many centuries" (Sabin 2014). With rapid developments in the area of clay additive manufacturing, there is an emerging possibility to reintroduce non-standard clay building blocks in load bearing applications. The motivation for such research trajectories comprise of "a qualitative, design driven desire for novel forms, or an aspiration for the quantitative improvement of building performance metrics" (Seibold et al. 2018). However, literature outlining expansive utilization of these technologies within comprehensive processes of algorithmic generation, manufacturing, digital and physical evaluation, and architectural application remains lacking.

As part of comprehensive workflow for PolyBrick 2.0, novel algorithmic processes are developed, fabrication methods are outlined, prototype performances are evaluated, and architectural applications are envisioned. Hence, PolyBrick 2.0 suggests a complete methodology in continuing PolyBrick's ubiquitous aim to "bridge digital processes with the production and design of nonstandard ceramic building blocks in architecture" (Sabin et al. 2014). Within this process the role of "non-standard" components in load bearing applications is addressed and the duality of solidity and porosity in relation to structural performance is explored.

BACKGROUND

Several projects with similar premises of load-bearing application in relation to clay/ceramic additive manufacturing technologies (AMTs) have emerged over the past decade. Robotically fabricated clay column introduced by Ana Anton and Ahmed Abdemahgoun as part of Digital Building Technologies in ETH Zurich is one of such projects. Anton et al. make use of robotically manufactured, non-standard clay components and attribute possibilities of load bearing in their contextualization of these components as a column (Anton and Abdelmahgoub 2018). With their proposal for a prototypical pavilion in CEVISAMA 2017, Seibold et al. also explore architectural load bearing possibilities created by 3D printed unique clay components.

Expanding upon complex geometrical possibilities and non-standardization realized by AMTs, several projects acknowledge trabecular bone structure as an applicable biological precedent. Alvin Huang's ***Durotaxis Chair*** (Huang 2016) and Baerlecken et al.'s ***Osteotectonics*** (2015) recognize unique mechanobiological characteristics of trabecular bone within various possible design applications. ***Osteotectonics*** offers the trabecular structure as a weight-efficient specialized strategy in its reinterpretation as structural nodes. ***Durotaxis Chair*** serves as an example of algorithmically established strategical porosities inspired by the trabecular geometry in increasing material efficiency within load bearing application (Huang 2016). Other projects, such as mechano-adaptive space frame generation workflow by Felder et al. (2016) and Naboni's analyses on Lattice-base cellular solids (Naboni et al. 2017) show advantages of adaptive, algorithmically generated lattice structures in the realm of load bearing.

PolyBrick 2.0 strives to heighten the precision and breadth of workflows within the literature of clay/ceramic AMTs through proposed methodologies. The outlined processes include bio-integrative research, algorithmic modeling and meshing strategies, physical and digital prototyping and evaluation, and suggestions of design possibilities. As part of the bio-integrative research phase, our team draws from expansive structural knowledge present in the natural precedent of the bone categorized and outlined in the following sections.

Morphological Formation and Quantifiers

Like many natural load-bearing structures, the bone is comprised of a solid outer shell and a foam (cancellous) core (Torres et al. 2016). The cancellous core is a heterogeneous lattice structure and is quantified by the morphological parameters of tissue volume (mm^3), bone volume (mm^3), bone volume to tissue volume ratio, trabecular number (per mm), trabecular thickness (micrometers), trabecular separation (micrometers), trabecular connectivity (per mm^3) (Bagi, Berryman, Moalli 2011) (Appendix 1). These parameters are reinterpreted and implemented algorithmically as part of the first step of our workflow.

Transformation Through Responsive Adaptability

The trabecular bone exhibits morphological responses to applied loading conditions. These morphological responses include bone resorption and apposition, and trabecular directionality adaptations. "Bone is a dynamic tissue that is normally renewed through balanced bone resorption and apposition processes that are choreographed in space and time" (Chen et al. 2010). Trabecular thickness, hence, can be regarded as proportional to applied cyclic stress stimuli. Additionally, directional transformations are observed within the bone whereby trabeculae are "oriented in the direction of the compressive load applied" (Tsubota et al. 2009). In short, directional transformations occur such that each trabeculae is carrying loads in its strongest axis. These adaptations establish the trabecular lattice as an ever-evolving function of specific loading conditions (Appendix 2).

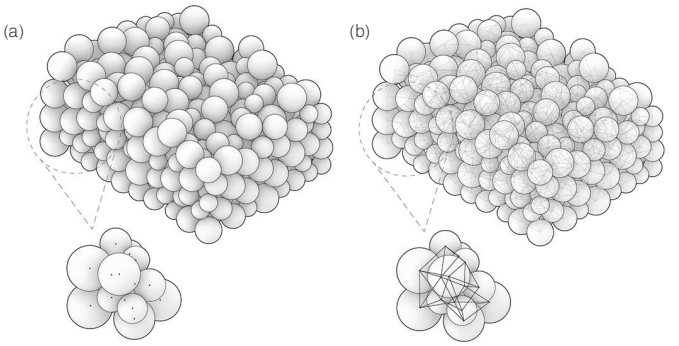

2

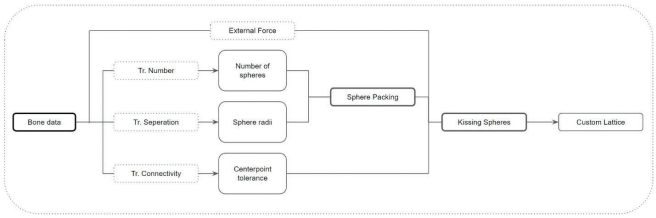

3

2 Diagrammatic representation of the initial sphere packing (a) followed by lattice generation through the employment "Kissing spheres" algorithm (b)

3 Workflow diagram with initial sphere packing algorithm consisting of interpretation of trabecular number and trabecular separation parameters as sphere number within a bounding box and sphere radii, respectively as marked

The outlined biological precedent of the trabecular bone provides framework for PolyBrick 2.0 to rethink building technologies with considerations of responsiveness and material efficiency.

METHODS

PolyBrick's algorithmic framework occurs in two scales: local and global. The specific workflows pertaining to these two scales are detailed in the following categories. In the first category—describing local (lattice) scale workflows—the algorithmic generation of the PolyBrick geometry is outlined. This is followed by the introduction of working methodologies for physical and digital performance testing. In the second category—describing universal (architectural) scale workflows—architectural applications of PolyBrick are proposed and case specific loading responses and tessellation methods are described.

Local (Lattice) Scale

This phase is initiated through the algorithmic interpretation of the trabecular bone's morphological quantifiers outlined in the Background. Morphological quantifiers of interest are determined as trabecular number, trabecular thickness (micrometers), trabecular separation (micrometers), and trabecular connectivity (per mm^3).

Sphere Packing: Algorithmic Interpretation of Tr. Number and Tr. Separation

Digital interpretation of morphological quantifiers of trabecular bone is achieved through the implementation of a sphere packing algorithm. This allows for a translation of trabecular number and trabecular separation, whereby trabecular number is interpreted as the number of spheres present within a predetermined bounding box, and trabecular separation is interpreted as the range of sphere radii determining the distances between sphere center points. Sphere centers, hence, are regarded as the algorithmic interpretation of nodal points (Figure 2(a)). The pseudocode of this workflow is presented in Figure 3.

Algorithmic employment of sphere packing is first realized with the aid of Kangaroo, a Grasshopper plug-in for Rhinoceros 6.0. Kangaroo allows for a sphere packing process within a set bounding box (Appendix 3). However, due to lack of precision in aspects of radius distribution and sphere number, this plug-in is then replaced by a custom C#-based sphere packing. For this, a bounding geometry is modeled in Rhinoceros 6.0 and linked to the custom C# Grasshopper plug-in. This script generates an initial sphere within this bounding geometry and new spheres are iteratively added and relaxed after checking for collisions. This is continued until the bounding geometry is full. The process is expedited by a virtual 3D grid where the cell sizes are slightly larger than the largest sphere packed within the bounding box, which decreases the number of locations checked for collisions (Appendix 4). This custom C# algorithm allows for heightened control in the bounding condition and sphere distribution.

After the sphere packing process, a corresponding lattice is generated where the centers of touching spheres are connected. The lattice geometry is generated in accordance with the prevalent force flows inside the spheres in their packed state (Figures 4a,b). This step is achieved through a secondary custom C# script incorporated as a Grasshopper component.

Local Lattice Thickening: Algorithmic Interpretation of Trabecular Thickening and Wolff's Law

The sphere packing lattice is uniformly thickened using Autodesk's T-Splines function in Rhino (Figures 4b,c). This allows for digital and physical performance evaluation of changing lattice geometry parameters (sphere radii and connectivity) while maintaining a controlled uniform thickness parameter. .

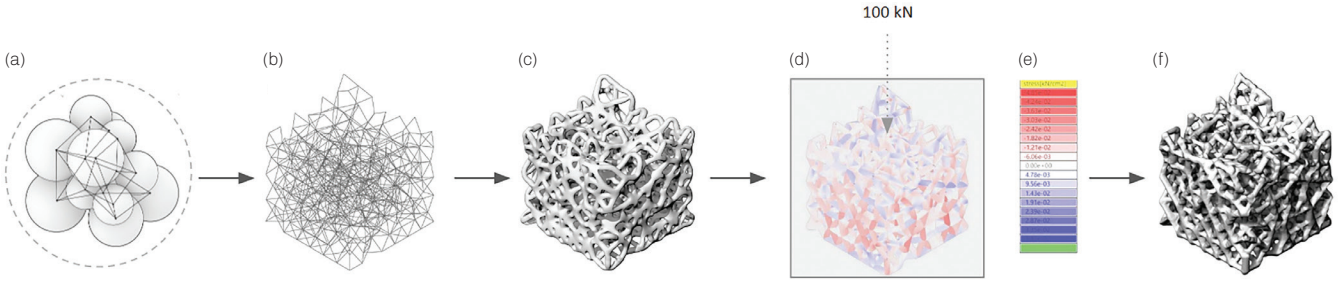

4 Process diagram from the stage of lattice generation (a-b) to uniform thickening; (c) Illustrated is a workflow whereby a bounding box of 38 mm x 38 mm x 38 mm is packed with uniform spheres of 3 mm radii, the resulting lattice beams are then thickened uniformly by 1.5 mm in radius. A theoretical lateral load of 100 kN is then applied to the lattice system; (d) The resulting stress values are calculated (e) along strut lengths; Thickening values are established as a direct function of these varying stress values and realized through a Cocoon based Grasshopper script (f)

Microscale adaptations within the strut surface, in accordance with the prevalent varying stress values, is foreseen as an additional step to increase material efficiency. Through application of Wolff's law and load specific local absorption/resorption processes in the trabeculae at the scale of an individual strut, our team strives to achieve similar local load specificity in the employed thickening algorithms. Generated lattices of 38 mm x 38 mm x 38 mm dimension are digitally analyzed under a preset uniform compressive loading condition (100 kN total). Karamba for Grasshopper is used to extract axial force values from the lattice. Lattice struts with higher corresponding axial stress values are thickened proportionally with the aid of the *Cocoon* plug-in for Grasshopper. Hence, thickening values are determined as response functions of specific local stress values along individual beams (Figures 4c,d,e).

Directionality Adaptations

Directional responsiveness to effective loads is foreseen as a second method to increase efficiency (Figure 5). As observed in the natural bone model, the trabecular structure is oriented parallel to the load direction. In the algorithmic interpretation of this phenomena, the PolyBrick workflow is expanded with the addition of a 3D ellipsoid packing algorithm in which the main principal axes of packed ellipsoids are aligned with the load directionality (Appendix 5).

The initial ellipsoid packing workflow is established using a MATLAB algorithm. The pseudocode for this workflow is outlined in Appendix 6. This algorithm expands upon the previously outlined sphere packing algorithm with the addition of more complex collision detection. The ellipsoid packing algorithm uses a standard rotation matrix (R) to reorient the ellipsoids to the global 3D Cartesian coordinate system and to calculate the distance between their centers. As part of realizing the collision detection, a "small angle assumption" is employed. Adjacent ellipsoids are assumed to have a small angle in between (with similar axial direction) because the angle between the principle stress directions in adjacent locations varies within a small range. By calculating the center distance of two ellipsoids and their rim distance along this direction we derive their collision state (Figure 6). Building upon the continuous algorithmic workflow, this step is also formalized as a C# based Grasshopper component, and compiled as part of the PolyBrick plug-in.

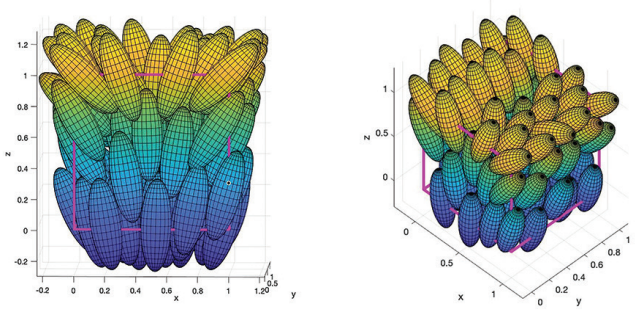

5

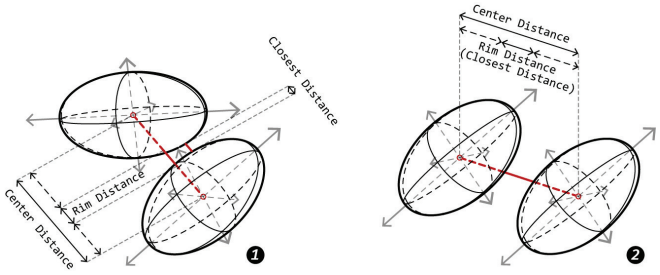

6

5 MATLAB based ellipsoid packing visualization: Ellipsoids are oriented towards the maximum principal stress direction on their larger axis, to increase structural capacity of the system by responding to directionality

6 (1) Closest distance is hard to calculate when two ellipsoids are not close to parallel; (2)" Small angle assumption" simplifies the calculation of the closest distance of two ellipsoids

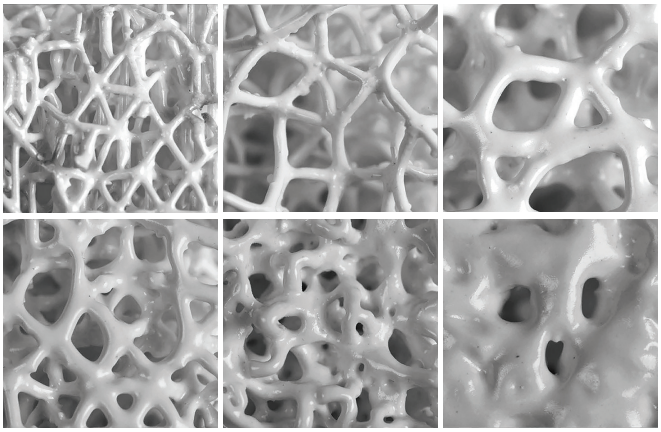

7

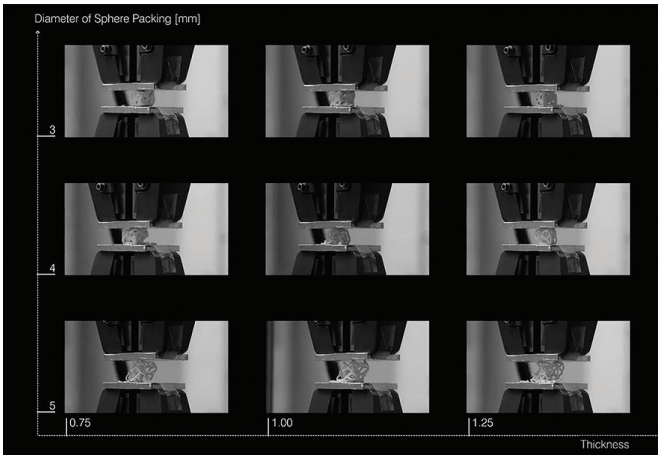

8

7 Close-up images of the physical prototypes showing the spatial and architectural possibilities created through varying levels of porosity present in PolyBrick 2.0 geometries

8 Snippet from the video recording of Instron compressive tests of the Kangaroo based sphere packing prototypes

In foreseeing the three-dimensional global scale application of this algorithm, data derived from ANSYS based tests at 1:1 scale are used to guide directional responses of ellipsoid axes. ANSYS data contains a grid, in which each node of the grid has maximum principal stresses, middle principal stresses, minimum principal stresses, and their respective directions (either two are perpendicular). The ellipsoids are rotated by their position in this grid, in correspondence to the directions of three axes to the interpolated maximum, middle, and minimum principal stress directions on its centroid.

PHYSICAL PROTOTYPING AND MECHANICAL PROPERTY TESTING

Ceramic 3-D Printing

Building upon extensive prior research, Polybrick 2.0 continues a rigorous exploration of ceramics and respective innovative fabrication methodologies. In moving from algorithmic generation to physical prototyping, eighteen 38 mm x 38 mm x 38 mm cubic prototypes are printed for documentation (Figure 7) and eighteen 25.4 mm x 25.4 mm x 25.4 mm cubic prototypes are printed for mechanical testing. For all listed prototypes Formlabs Form 2 3D printers are utilized with Formlabs UV curing ceramic resin.

Proceeding printing and support removal, all prototypes are bisque fired at cone setting 06 with medium speed to burn out resin material.The prototypes are then glazed and kiln fired using cone setting 4 and medium speed. In all cases, an average of 9.6 percent shrinkage is observed between the greenware and bisque fired prototypes (Appendix 7). In order to account for this shrinkage, custom settings suggested by the "Preform" software are followed and the prints are scaled up by a factor of 1 to 1.123.

Based on observational shrinkage data, a 1.52% discrepancy between the recommended shrinkage rate and the actual shrinkage is recorded (Appendix 8).

Mechanical Testing

Proceeding the compilation of outlined algorithmic structures that generate PolyBrick prototypes, frameworks for comparative mechanical performance analysis are established. For this, both digital and physical means of analysis are used as outlined in the following sections.

Physical Compressive Buckling Testing

Physical compressive buckling testing is carried through to record mechanical properties of strength, stiffness, first failure force, and peak failure force, and failure displacement associated with generated PolyBrick lattices. It is predicted that the implementation of a custom code-based algorithm that enhances control parameters will directly translate to enhanced mechanical performance.

Nine cubes are generated with Kangaroo-based sphere packing and C#-based sphere packing algorithms respectively, with varying control parameters of sphere size and strut thickness. The prototypes are printed with Formlabs Form 2 ceramic resin printing technologies, treated as described in the previous section "Ceramic 3-D Printing", and tested for compressive buckling performance using an Instron Universal Hydraulic Tester (Figure 8). A solid cube with the same bounding proportion is tested as a control (Appendix 9). For all tests first failure load (N) and maximum failure load (N) points are recorded and stiffness is derived.

Through this testing, a framework for the comparison of mechanical properties between two algorithmic approaches (Kangaroo and C#-based sphere packing) and general performance evaluation of proposed porous brick

geometries established and compared to corresponding solid prototypes.

Digital Compressive Buckling Simulation Testing

With use of finite element analysis (FEA) tools, a system for continuous digital mechanical performance analysis is achieved. This is a means to streamline accurate digital mechanical performance analysis prior to physical prototyping. The digital FEA tool ANSYS is employed as a means of lattice testing under standard uniform loading. The same set of prototypes analyzed under physical compressive buckling testing are simulated digitally. The results pertaining to strength, stiffness, first failure force, and first failure displacement are compared to the results obtained from physical compressive buckling testing. This is to determine the accuracy of employed testing methods and note discrepancies which may occur due to printing and/or physical testing inaccuracies. Through efforts to establish accurate digital means of evaluation, we aim to provide designers with a user-friendly and streamlined toolset for digital generation and evaluation of PolyBrick architectures.

Global Stress Magnitudes and Responsive Sphere Packing

After generating and testing the mechanical performances of speculative PolyBrick 2.0 prototypes with varying properties of packing density (sphere radii input) and strut thickness, global scale applications and architectural possibilities are proposed. Stress magnitudes and flows in preset loading scenarios at the architectural scale are analyzed and PolyBrick geometries are refined accordingly (Figure 9). For this, FEA programs such as ABAQUS and ANSYS are utilized.

With the use of global finite element analysis, the aim is to achieve responsive lattice heterogeneity at the architecture scale according to prevalent stress magnitude and direction data. To initiate this process, a hypothetical loading condition is applied upon a speculative wall with the dimensions of 0.2 m x 2 m x 3 m. This loading condition includes transferred wind loads of 40 kg/m^2, a point load of 3100 kg, and the wall's self-weight (Figure 10). Data pertaining to stress magnitudes in this described loading condition is obtained via ANSYS and visualized through a colored mesh where a color value is assigned to a corresponding stress magnitude. Previously outlined C# sphere packing algorithm is refined to determine sphere diameter distribution based on these mapped global stress magnitudes. Larger spheres are packed in areas with lower stress and small spheres in areas with higher stress.

Global thickening is another response parameter to the global stress magnitude data. Mechanical and digital testing show that both sphere radii and strut thickness influence structural performance. Thickness variation across the global geometry in correspondence with pertaining stress magnitude is possible. Either one can be emphasized by the designer based on programmatic needs. The other is then to be calculated accordingly based on stress magnitude, using the relationship: ***(Thickness/ Radius) x Factor***, where the *Factor* is to be calculated based on physical tests. Control within parameters of sphere radii distribution and strut radii distribution gives the designer flexibility in responding to unique programmatic and performance needs.

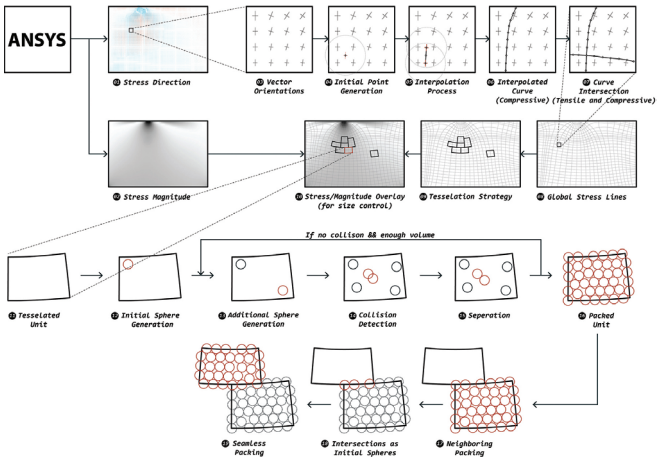

9 Full-scale workflow: Stress direction(01) is used to interpolate compressive and tensile curves (07) that form global stress lines(08), which are then overlaid with the stress magnitude data (08) to form a speculative tessellation(10). Tessellated units are then individually packed (11) using our custom algorithm and intersection points (18) are utilized to achieve a seamless packing (19).

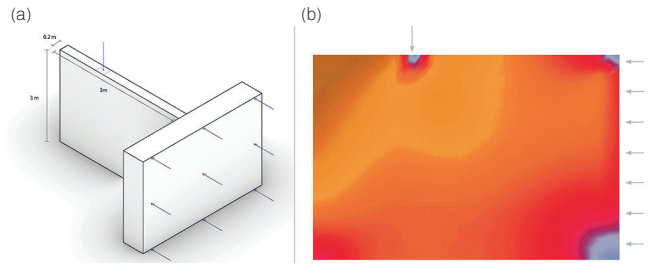

10 (a) Speculative wall condition with transferred wind loads of 40 kg/m2, a point load of 3100 kg and self- weight were applied. (b) Generated colored mesh with color values correlating to stress magnitude date extracted from ANSYS simulation.

Global Stress Distribution
and Case Specific Tessellation

While stress magnitudes serve to inform a responsive sphere packing and thickening algorithm, stress directionalities are foreseen as important drivers of tessellation speculations. Using the vector directionality data obtained from ANSYS, a custom algorithm is generated to derive the principal stress lines. Building upon the premise that principle stress lines "(...) are pairs of orthogonal curves that indicate trajectories of internal forces (...) [that] naturally encode the optimal topology" (Tam and Mueller 2015), the derived lines are utilized as guides to trace brick boundaries (Figure 9 (01-08), Appendix 10).

Brick sizes are constrained to the dimension of the available kiln (61 cm in diameter) to ease both digital and physical fabrication. Hence, the bounding condition of each brick geometry is manually assigned using the boundaries of the previously derived principle stress lines (Figure 9 (09). Areas with lower magnitudes of stress—thus larger sphere radii—utilize the maximum dimensions within the 61 cm constraint, whereas areas of larger magnitudes of stress are populated with smaller bricks (Figure 9 (10)).

Packing each brick individually post-tessellation generates a new problem of potential discontinuities between bricks. Our C# sphere packing algorithm is refined once more to input spheres located at tessellation boundaries as a starting condition for neighboring bricks. Each respective brick is packed in correspondence to its neighbors (Figure 9(18-19)).

RESULTS

Workflow

A comprehensive workflow is developed, entailing algorithmic generation of PolyBrick lattices and corresponding reevaluation and adaptations according to local and global scale stress distributions. The algorithmic process is formalized as a custom Grasshopper plug-in containing components for sphere packing, ellipsoid packing, lattice generation (kissing spheres), and thickening meshing (Appendix 11) applicable to various global geometries. Additionally, formalized frameworks for digital and physical performance analysis are initiated, tessellation logics are outlined, and several design speculations are presented.

Performance Testing

Several parameters are foreseen to impact structural performance (covered in detail in previous sections). These parameters include strut thickness andresponsive thickening (1), sphere packing density (sphere radii input) (2), and lattice directionality (3) based on global stress direction input. The respective effects of these parameters on brick performance are evaluated through digital and physical tests.

Physical compressive testing is performed on nine Kangaroo based sphere packing lattices and nine C# based sphere packing lattices. Failure loads (Figure 11) are recorded and stiffness is derived based on peak failure points. Aforementioned parameters of sphere radii input (1) and strut thickening (2) are analyzed in relation to performance. It is observed that thicker struts and smaller sphere radii amount to increased first and peak failure force (N) and increased stiffness (Figure 12). All PolyBrick prototypes show multiple peak loading values. This is a general characteristic of cellular solids and indicates multiple strut/member breakages before catastrophic failure (full destruction of prototype). Higher energy absorption and a longer life span can be foreseen in PolyBrick prototypes compared to the solid cube prior to catastrophic failure.

Preliminary material efficiency calculations are done by dividing stiffness (N/mm) by average effective volume (mm3). This is to understand the benefits of PolyBrick prototypes compared to solid geometries of the same material. For the solid control cube, stiffness/effective volume is calculated as 0.75 N/mm^4. The C# based prototype with 4mm sphere radii input and 1.25 mm strut thickening is chosen for comparison because it achieves the highest stiffness of PolyBrick geometries tested. The stiffness per effective volume of this prototype is 0.79 N/mm^4. This shows that Polybrick geometries provide some advantage of mechanical performance per volume.

Although the lattice directionality parameter (3) is not tested physically, it is expected to play an important role in decreasing average cross sectional area perpendicular to loading and thus increasing material efficiency. Simulation testing via ANSYS is performed to compare the performance of lattice structures with varying directionality trends. Among the four simulated cubes, the cube with vertical directionality to applied loading shows largest failure force reaching 594.89 N (Appendix 12). This supports the premise of increased load capacity and material efficiency through processes of directional alignment.

Comparison: Physical Compressive Buckling Testing and Digital Compressive Buckling Testing

Results obtained from the compressive buckling simulation testing are graphed in comparison to those obtained from Instron compressive buckling testing (Appendix 13). The stiffness and strength are normalized by the

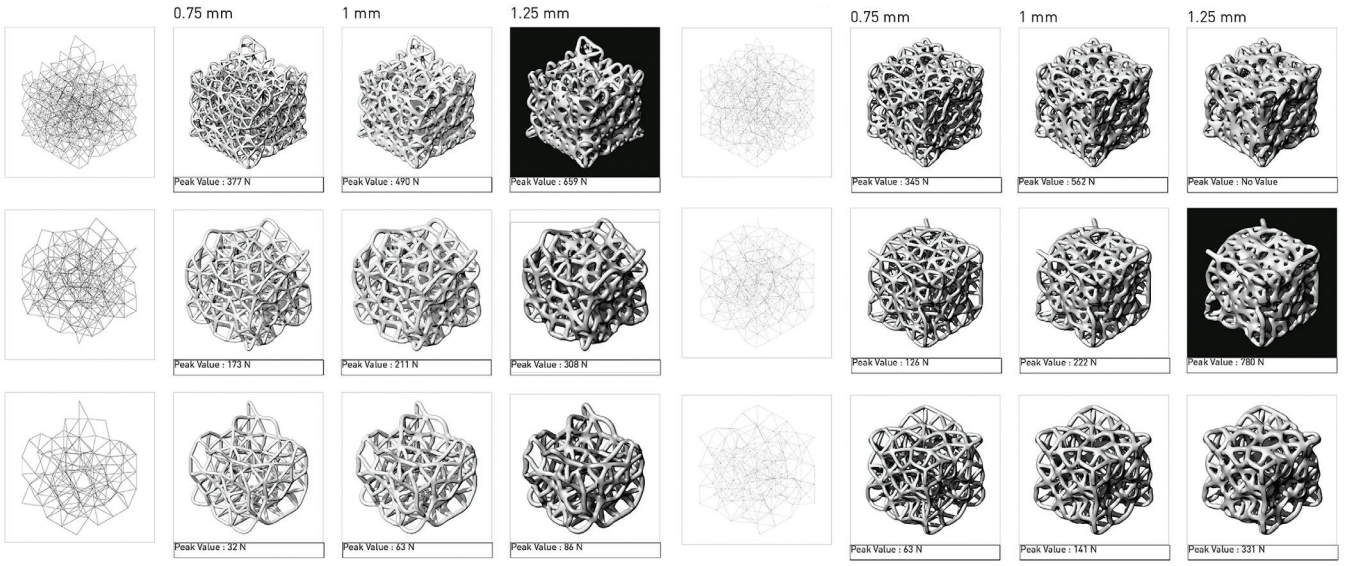

11

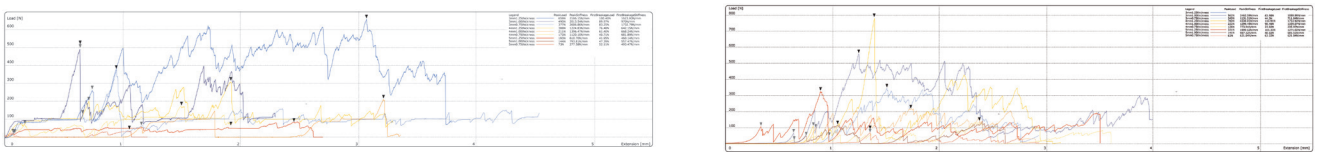

12

11 Peak force (N) values for models that are generated using the Kangaroo based sphere packing (left) and C# based custom sphere packing lattices (right); Generated prototypes vary in sphere radii and strut thickness, and in both cases increasing strut thickness and decreasing sphere radii amount to increased peak load value

12 Load (N); Displacement (mm) curves for Kangaroo based sphere packing (left) and C# based custom sphere packing lattices (right); C# based sphere packing lattices have higher peak load values (N) and derived stiffness values (N/mm) as recorded; Derived stiffness values are used to calculate material efficiency for comparison between PolyBrick and solid cube prototypes

apparent density of the samples. The strength to density ratio is plotted against the stiffness to density ratio. The data attempts to compare the performance predicted by the simulation to the real sample. The strength to weight and stiffness to weight ratios of the samples increase with strut diameter according to both the simulation and experiment. The simulation and experiment show different trends for lattice spacing. The experiments suggest that a larger lattice spacing will result in a higher stiffness to weight ratio, but a lower strength to weight ratio. Increased accuracy in both physical and digital simulation testing is necessary to refine these findings and establish reliable analysis methodologies. This an important future direction.

Full Scale Speculation

A full scale architectural speculation is proposed following outlined tessellation and packing strategies. This speculation is based on stress magnitude and directionality parameters derived from global scale ANSYS simulations with previously outlined loading conditions. Sphere packing density and tessellation boundaries are generated as direct functions of mentioned stress magnitude and directionality data. The resulting wall is porous, responsive to its specific loading conditions, and lightweight. Several bricks of this tessellation are printed at quarter scale for preliminary assembly visualization (Figure 13). The tessellated and packed wall is digitally visualized in Figure 14.

Several further diagrammatic speculations of PolyBrick applications on more organic/curved architectural bodies are investigated (Figure 15).

DISCUSSION

Results Evaluation

Preliminary calculations suggest PolyBrick geometries have potential to improve upon material efficiency rates (stiffness/effective volume) of corresponding solid geometries. Such results are promising in achieving our goal of lightweight and material efficiency while maintaining high mechanical performance. Hence, ceramic building blocks re-enter the canon of architectural load bearing technologies with increased porosity and load responsiveness.

While architectural potential and high material efficiency are observed, a larger sample is needed to increase the

accuracy of data relating to mechanical performance. This can create a useful archival reference for the future analysis and employment of PolyBrick geometries at the architectural scale. Additional testing is needed for ellipsoid packing based directional prototypes.

There is some remaining discrepancy between the physical testing and simulations. Larger sample sizes in physical testing and increased accuracy in ANSYS modeling are foreseen as future trajectories in addressing this.

Limitations

Algorithmic limitations pertain to the need for high computation power and time. Similarly, ceramic resin printing processes are constrained by fabrication time and the print bed size (145 mm x 137 mm x 175 mm). In addition, larger prototypes take several days to weeks to print. Ceramic resin pricing is also indicative of a costly process when envisioning larger scale applications. Material constraints largely pertain to unique material properties of 3D printed ceramics. Because of its natural porosity and low-density, the mechanical properties of 3D printed ceramic prototypes are difficult to analyze. Multiple tests are required to record accurate data pertaining to comparative mechanical performances. In addressing listed limitations, we are investigating following future trajectories:

1. Customized meshing strategies to maximize computation time and speed

2. Investigation on robotic clay extrusion as a potential tool for larger scale fabrication

3. Investigation of performance evaluation discrepancies between simulation and physical testing

4. Implementation of more advanced testing methodologies for accurate material efficiency conclusions and print accuracy evaluations through possible scanning processes

CONCLUSION

We expand upon pursuits to implement additive manufacturing tools (AMTs) in revitalizing ceramic load bearing structures in more materially efficient and responsive contexts. A precise and complete workflow is outlined and formalized as a Grasshopper plug-in, “PolyBrick,”

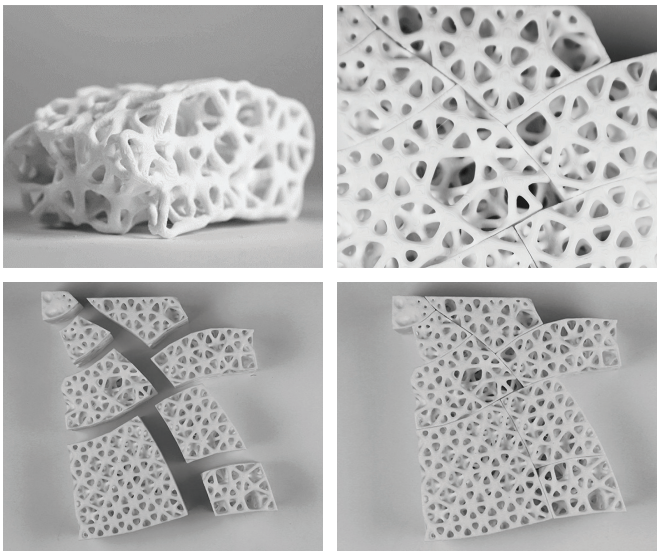

13

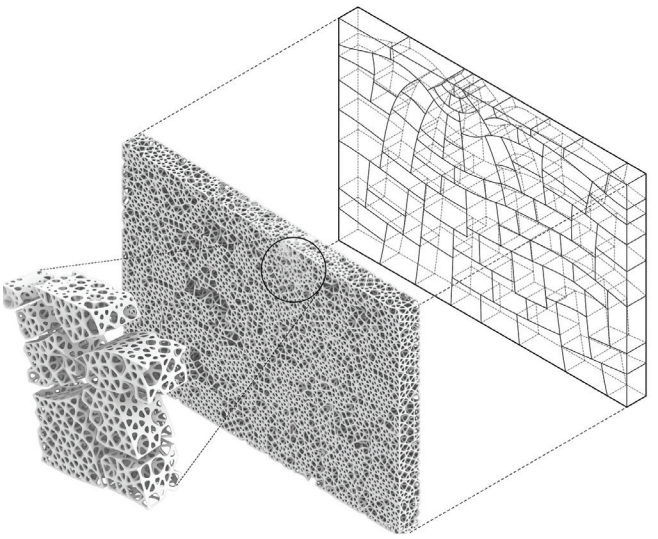

14

15

13 (top left) Prototype of one brick tessellation component from suggested speculative wall: the boundary condition of the brick component corresponds to the principle stress lines; (top right) Zoomed in shot of tesselation boundaries; (bottom) Model illustration of assembly process possibility

14 Digital representation of full scale wall proposal based on aforementioned loading condition

15 (left) Diagrammatic PolyBrick Lattice in curved geometry; (middle) Applied lattice thickening visualized digitally; (right) 3D printed diagrammatic model

accompanied by a custom C# tessellation algorithm is established for further implementation by users and designers. The trajectory of the research introduces a design process emphasizing adaptability and lightweight, with various potential strategies that relate to environmental responsiveness and programmatic concerns.

We follow a rigorous process of performance analysis with potential to be implemented in future workflows incorporating AMTs. Outlined processes of evaluation strengthen the argument for the implementation of non-standard, porous ceramic building components as a viable material for load bearing/architectural application. Hence, PolyBrick offers a non-standard, light weight, and efficient load bearing material system alternative to current construction methodologies. The integral role of porosity opens up potential for further design exploration and integration of additional material systems.

ACKNOWLEDGEMENTS

This research was generously supported by the Sabin Lab and Sabin Lab personnel at the College of Architecture, Art, and Planning, Cornell University. We thank Jenny Sabin for her support and advising, Sabin lab personnel, in particular David Rossenwasser for continued support, and Christopher J. Hernandez for offering valuable consultation and expertise.

REFERENCES

Anton, A., and A. Abdelmahgoub. 2018. "Ceramic Components - Computational Design for Bespoke Robotic 3D Printing on Curved Support." In Computing for a Better Tomorrow; Proceedings of the 36th eCAADe Conference, Volume 2, 71-78.

Baerlecken D. and S. Gokmen. 2015. "Osteotectonics: Trabecular Bone Structures and Their Adaptation for Customized Structural Nodes Using Additive Manufacturing Techniques." Real Time: Extending the Reach of Computation; Proceedings of the 33rd eCAADe Conference, Material Studies, Volume 2, 439-448.

Bagi, C.M., E. Berryman, and M.R. Moalli. 2011. "Comparative Bone Anatomy of Commonly Used Laboratory Animals and Implications for Drug Discovery." CompMed 61(1): 76-85.

Bilotti, J., B. Norman, D. Rosenwasser, J. Leo Liu, and J. Sabin. 2018. "Robosense 2.0. Robotic sensing and architectural ceramic fabrication." In ACADIA 18: Recalibration; On Imprecision and Infidelity; Proceedings of the 38th Annual Conference of the Association for Computer Aided Design in Architecture, 276-285.

Chen, J.H., C. Liu, L. You, and C.A. Simmons. 2010. "Boning up on Wolff's Law: Mechanical regulation of the cells that make and maintain bone." J. Biomech 43(1): 108-118.

Felder, A., H. Lewis, D. Piker, A. Pereira, and X. De Kestelier. 2016. "Mechano-adaptive space frame generation based on ellipsoid packing." In Proceedings of the IASS Annual Symposium 2016: Spatial Strutures in the 21st Century, edited by K. Kawaguchi, M. Ohsaki, and T. Takeuchi. Tokyo, Japan.

Garcia, A.P., and F.G. Martinez. 2009. "Natural structures: Strategies for geometric and morphological optimization." In Proceedings of the International Association for Shell and Spatial Structures (IASS) Symposium. Editorial Universitat Politècnica de València. http://hdl.handle.net/10251/6955.

Hernandez, C.J., G.S. Beaupre, and D.R. Carter. 2000. "A model of mechanobiologic and metabolic influences on bone adaptation." Journal of Rehabilitation Research and Development 37(2): 235-244.

Huang, A. 2016). "From Bones to Bricks." In ACADIA 2016: Posthuman Frontiers: Data, Designers, and Cognitive Machines, Proceedings of the 36th Annual Conference of the Association for Computer Aided Design in Architecture, 318-325.

Naboni, R. and A. Kunic. 2017. "Design and Additive Manufacturing of Lattice-based Cellular Solids at Building Scale." In SIGraDi 2017, XXI Congreso de la Sociedad Ibero-americana de Gráfica Digital 3(12): 369-375.

Sabin, J., M. Miller, N. Cassab, and A. Lucia. 2014. "PolyBrick: Variegated Additive Ceramic Component Manufacturing (ACCM)." 3D Printing and Additive Manufacturing 1(2): 78–84. doi:10.1089/3dp.2014.0012.

Seibold, Z., K. Hinz, J.L. García del Castillio y López, N. Martínez Alonso, S. Mhatre, and M. Bechtold. 2018. "Ceramic Morphologies; Precision and control in paste-based additive manufacturing." In ACADIA 18: Recalibration: On Imprecision and Infidelity; Proceedings of the 38th Annual Conference of the Association for Computer Aided Design in Architecture, 350-357.

Tam, K.M.M. and C.T. Mueller. 2015. "Stress Line Generation for Structurally Performative Architectural Design." In ACADIA 15: Computational Ecologies: Design in the Anthropocene; Proceedings of the 35th Annual Conference of the Association for Computer Aided Design in Architecture, 95-109.

Torres, A.M., J.B. Matheny, T.M. Keaveny, D. Taylor, C.M Rimnac, and C.J. Hernandez. 2016. "Material heterogeneity in cancellous bone promotes deformation recovery after mechanical failure." Proceedings of the National Academy of Sciences 113(11): 2892-2897.

Tsubota, K., Y. Suzuki, T. Yamada, M. Hojo, A. Makinouchi, and T. Adachi. 2009. "Computer simulation of trabecular remodeling in human proximal femur using large-scale voxel FE models: Approach to understanding Wolff's law." J. Biomech 42(8): 1088-1094.

IMAGE CREDITS

Appendix 1: © Bagi CM, Berryman E, Moalli MR. (2011). "Comparative Bone Anatomy of Commonly Used Laboratory Animals and Implications for Drug Discovery". CompMed, 61(1), 76-85
Appendix 2: © Tsubota K, Suzuki Y, Yamada T, Hojo M, Makinouchi A, Adachi T. (2009). "Computer simulation of trabecular remodeling in human proximal femur using large-scale voxel FE models: Approach to understanding Wolff's law". J Biomech, 42(8), 1088-1094
All other drawings and images by the authors.

Eda Begum Birol is an undergraduate a B.Arch student at Cornell University and a research associate in the JSLab.

Yao Lu is a graduate pursuing a M.S.MDC from Cornell University and a research associate with the JSLab. He holds a B.Eng and M.Arch from Tongji University.

Ege Sekkin is an undergraduate a B.Arch student at Cornell University with additional background in computer science and graphics.

Colby Johnson is an undergraduate student pursuing a B.S in Mechanical Engineering from Cornell University, and a Research Associate with JSLab. Johnson has engaged in biomechanical design research.

Yaseen Islam is a recent graduate with B.S. in Mechanical Engineering from Cornell University and a collaborator on PolyBrick 2.0 research. Islam has engaged in biomechanical design research and mechanisms and product development.

David Moy is a recent graduate of Master of Engineering in Mechanical Engineering from Cornell University. He is a collaborator on PolyBrick 2.0 research, assisting with predicting the mechanical properties of polybricks using FEA.

Jenny Sabin is the Arthur L. and Isabel B. Wiesenberger Professor in Architecture and Director of Graduate Studies in the Department of Architecture at Cornell University where she established a new advanced research degree in Matter Design Computation. She is principal of Jenny Sabin Studio, an experimental architectural design studio based in Ithaca and Director of the Sabin Lab at Cornell AAP.

APPENDIX

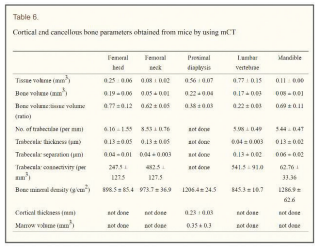

Table 6.
Cortical and cancellous bone parameters obtained from mice by using mCT

	Femoral head	Femoral neck	Proximal diaphysis	Lumbar vertebrae	Mandible
Tissue volume (mm^3)	0.25 ± 0.06	0.08 ± 0.02	0.56 ± 0.07	0.77 ± 0.15	0.11 ± 0.00
Bone volume (mm^3)	0.19 ± 0.06	0.05 ± 0.01	0.22 ± 0.04	0.17 ± 0.03	0.08 ± 0.01
Bone volume/tissue volume (ratio)	0.77 ± 0.12	0.62 ± 0.05	0.38 ± 0.03	0.22 ± 0.03	0.69 ± 0.11
No. of trabeculae (per mm)	6.16 ± 1.55	8.53 ± 0.76	not done	5.98 ± 0.49	5.44 ± 0.47
Trabecula: thickness (μm)	0.13 ± 0.05	0.13 ± 0.05	not done	0.04 ± 0.003	0.13 ± 0.02
Trabecula: separation (μm)	0.04 ± 0.01	0.04 ± 0.003	not done	0.13 ± 0.02	0.06 ± 0.02
Trabecula: connectivity (per mm^3)	247.5 ± 127.5	482.5 ± 127.5	not done	541.5 ± 91.0	62.76 ± 33.36
Bone mineral density (g/cm^2)	898.5 ± 85.4	973.7 ± 36.9	1206.4 ± 24.5	845.3 ± 10.7	1286.9 ± 62.6
Cortical thickness (mm)	not done	not done	0.23 ± 0.03	not done	not done
Marrow volume (mm^3)	not done	not done	0.35 ± 0.3	not done	not done

1

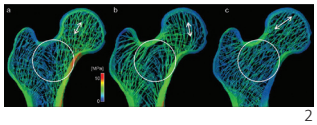

2

3

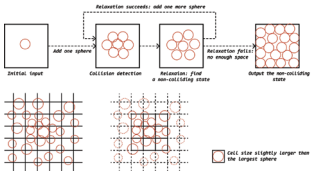

4

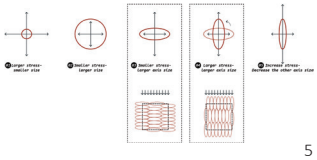

5

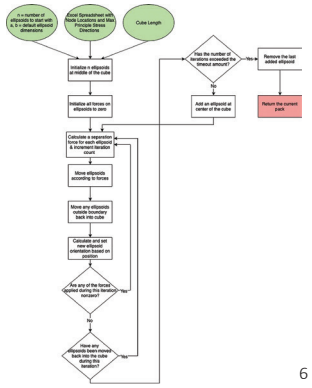

6

Test Cube		x dimension (mm)			y dimension (mm)			z dimension (mm)		
radius (mm)	thickness (mm)	Greenware	Bisque Fired	shrinkage (%)	Greenware	Bisque Fired	shrinkage (%)	Greenware	Bisque Fired	shrinkage (%)
3mm	0.75 mm	28	27	3.571428571	27	24	11.11111111	32	29	9.375
3mm	1.00 mm	29	26	10.34482759	28	24	14.28571429	31	24	22.58064516
3mm	1.25 mm	29	27	6.896551724	29	25	13.79310345	33	29	12.12121212
4mm	0.75 mm	27	26	3.703703704	28	25	10.71428571	32	28	12.5
4mm	1.00 mm	27	25	7.407407407	27	25	7.407407407	32	28	12.5
4mm	1.25 mm	29	25	13.79310345	29	26	10.34482759	33	32	3.03030303
5mm	0.75 mm	27	23	14.81481481	27	22	18.51851852	32	30	6.25
5mm	1.00 mm	28	25	10.71428571	29	27	6.896551724	32	31	3.125
5mm	1.25 mm	29	27	6.896551724	29	28	3.448275862	32	31	3.125
				8.68251941			10.72442174			9.40079559
									average shrinkage (%):	**9.602578914**

7

Sphere Radius	Strut Thickness		
3mm	0.75mm	1.00 mm	1.25mm
4mm	0.75mm	1.00 mm	1.25mm
5mm	0.75mm	1.00 mm	1.25mm

8

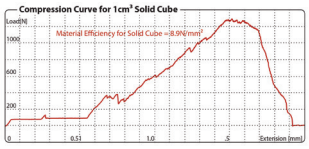

9

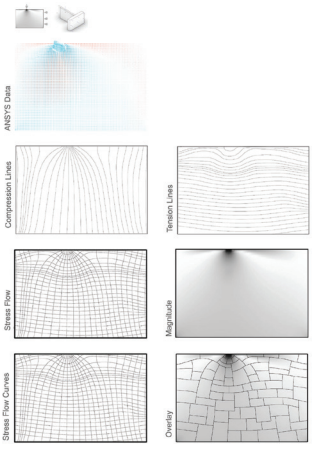

10

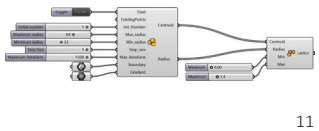

11

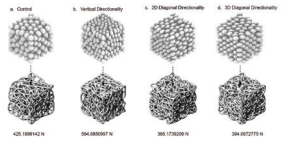

Directionality	Failure Force(N)
Vertical	594.8850997
2D-diagonal	394.0872775
3D-diagonal	388.1739209
Control	425.1899142

12

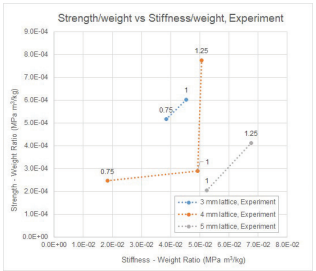

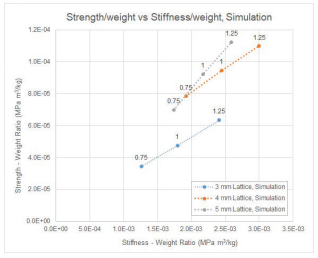

13

1 The two table serves to quantify the morphological characteristics of the trabecular bone of micemice. These quantifying parameters are obtained using micro CT scan technologies and are listed as tissue volume (mm3), bone volume (mm3), bone volume to tissue volume ratio, trabecular number (per mm), trabecular thickness (micrometers), trabecular separation (micrometers), trabecular connectivity (per mm3), bone mineral density (g/cm2), cortical thickness (mm), marrow volume(mm3). Through the establishment of a set series of morphological quantifiers, comparative analysis of bone microstructure inter and intraspecies is realized. Source: Comparative Bone Anatomy of Commonly Used Laboratory Animals: Implications for Drug Discovery (Bagi, Berryman, Moalli 2011).

2 Varying computed trabecular formations according to the directionality of the corresponding loading condition. While (b) and (c) present anisotropic trabecular formation following unidirectional loading conditions, (a) presents an anisotropic condition following a multidirectional loading condition, which is more similar to a real-life situation.Source: Computer simulation of trabecular remodeling in human proximal femur using large-scale voxel FE models: Approach to understanding Wolff's law (Tsubota et al. 2009)

3 General outline of a Kangaroo-based sphere packing workflow. An initial container is modeled using Rhinoceros 6.0. This container is linked to the Kangaroo-based Grasshopper script as a bounding box. Spheres of predetermined radii are then packed to fill the bounding box.

4 General outline of the code-based sphere packing workflow. An initial boundary geometry is modeled using Rhinoceros 6.0. This boundary geometry is linked to the C # Grasshopper script as a bounding volume. An initial sphere is then generated within the bounding box, and new spheres are added and relaxed after checking for collisions, until there is no more room to add another sphere(Top). The process is optimized by a virtual 3D grid of which the cell sizes are slightly larger than the largest sphere packed within the bounding box (Bottom). This way both the initial sphere generation and collision detection is quicker as only the adjacent 27 boxes have to be checked.

5 Reorientation and resizing of the struts using the new custom ellipsoid packing algorithm. Initial sphere packing algorithm dealt with larger stress values by assigning smaller radii (1-2). The ellipsoid packing algorithm aligns the long axis parallel to the larger stress direction to increase the number of struts in this direction (3-5).

6 Flowchart for 3D ellipsoid packing: *n* ellipsoids are initialized within a bounding box and forces are initialized. A separation force is calculated for each ellipsoid, and they are moved respective to the forces assigned. The iteration continues and new ellipsoids are added to the center until the "timeout" threshold is reached and the packing is returned.

7 Table 1: Shrinkage rates for the C# based test cubes.

8 Table 2: Outline of strut thickness and sphere diameter of printed nine Kangaroo and nine C# based prototypes. These prototypes were documented and tested using Instron Hydraulic Tester for mechanical properties.

9 Load (N) Displacement (mm) curve of solid control cube with dimensions 12 mm X 12 mm x 12 mm. Stiffness was calculated as 1296.31 N/mm based on this curve and used for further material efficiency comparisons.

10 Tessellation using stress flows and magnitudes: (top to bottom) Based on the speculative loading condition ANSYS data is extracted, this vector data is then used to map compressive and tensile forces, the intersection of these forces is then overlaid with an embedded stress magnitude mesh, which is then used to tessellate the geometry.

11 Custom "PolyBrick" plug-in. The input parameters consist of existing points as a tessellation strategy, initial number of packed spheres, max radii of spheres, min radii of spheres, step size, max iterations, boundary, and gradient mesh.

12 Test cubes with different directionalities, generated from ellipsoids: (a). control group showing our sphere packing algorithm, (b). ellipsoids oriented to respond to vertical directionality, (c). ellipsoids oriented to respond to 2D directionality, (d). ellipsoids oriented to respond to a real life like more complex loading condition.

13 Plot of experimental data obtained from Instron compressive buckling testing of the 12 code-based lattices (Right). Plot of the experimental data obtained from Ansys simulation testing of the 12 code-based lattice geometries (Left). The horizontal axis is the stiffness to weight ratio and the vertical axis is the strength to weight ratio. The strut diameters are labeled on the plots. The simulation and experiment both show that a higher strut thickness results in higher performance.